Design considerations for a compact proton beam writing system aiming for fast sub-10 nm direct write lithography

Xinxin Xu [a], Nannan Liu [a], P. Santhana Raman [a,b], Sarfraz Qureshi [a], Rudy Pang [a,b], Anjam Khursheed [b], Jeroen A. van Kan [a,*]

[a] Centre for Ion Beam Applications, Department of Physics, National University of Singapore, Singapore 117542, Singapore
[b] Department of Electrical and Computer Engineering, National University of Singapore, Singapore 117583, Singapore

ARTICLE INFO

ABSTRACT

In order to realize sub-10 nm feature size by proton beam writing (PBW) with writing speed comparable to electron beam lithography (EBL), a 200 kV compact PBW system is proposed here. In this system, a new nano-aperture electron impact ion source with a potential reduced brightness of 10^6 A/(m² srV) will be employed. To achieve sub-10 nm spot sizes with pA beam current, two different focusing lens configurations were evaluated. Both of these configurations were found to be theoretically capable of achieving sub-10 nm beam spot size.

© 2016 Elsevier B.V. All rights reserved.

1. Introduction

Proton beam writing (PBW) is a direct 3D writing lithographic technique that utilizes fast and focused MeV proton beam to pattern photoresists (e.g. hydrogen silsesquioxane (HSQ), SU-8, AR-P, and polymethyl methacrylate (PMMA)) and form sub-100 nm features [1,2]. This technique has been optimized at the Centre for Ion Beam Applications (CIBA), National University of Singapore [3,4], and has also been used at a few other ion microprobe laboratories worldwide (Leipzig [5], Lund [6], Ljubljana [7], Debrecen [8], Guildford [9], Rez [10], Takasaki [11], Tokyo [12], etc.). PBW is analogous to electron beam lithography (EBL), but employs protons with MeV energy. Fast protons traveling into materials mainly lose energy through proton-electron interactions. Due to the higher mass of the proton, when compared to the electron (~1800 times), MeV protons mainly transfer less than 100 eV energy to each secondary electron. As a result, there is limited scattering of protons and minimal lateral spread of secondary electrons in photoresists (e.g. less than 2 nm within 5 μm thick PMMA [13]), resulting in a minimized proximity effect coupled with a straight and deep proton trajectory. These features make PBW uniquely capable of fabricating high aspect ratio (height/width) sub 100 nm structures (~160 aspect ratio in SU-8 [3,14]) compared with other direct write litho-

graphic techniques. Since the depth of proton penetration in resist materials can be precisely controlled by varying the incoming beam energy, PBW can be used to fabricate multilevel structures in a single layer of resist [15,16]. Due to these prime features, PBW serves as a powerful tool in many applications, such as waveguide fabrication [17], micro and nano-fluidic device fabrication [18] and X-ray mask fabrication [19]. The PBW setup is also useful for 3D whole cell imaging and analysis [20]. Currently, the smallest structure that has been written with PBW is 19 nm lines in 100 nm thick HSQ using a 2 MeV proton beam [21]. Additionally, proton beam spot size down to 9.3×32 nm² has been achieved at CIBA [22]. The current PBW system in CIBA employs a radio frequency (RF) ion source [23] within a 3.5 MV High Voltage Engineering Europa Singletron™ accelerator [24]. Prior to entering the focusing system, the high energy proton beam is collimated using collimator slits. The focusing system consists of three magnetic quadrupole lenses (Oxford Microbeams OM52) operated in a spaced Oxford triplet configuration [25]. The RF ion source in the current PBW system has a reduced source brightness, B_r, of 20–30 A/(m² srV) [25], which is approximately 5 orders lower than a gallium liquid metal ion source [26] and 6 orders lower than an EBL system [27]. This lower brightness limits the writing speed, throughput, and the capability to further reduce the beam spot size in the current PBW system. To improve the writing speed and throughput of PBW, a 200 kV compact PBW (c-PBW) system aiming for single digit nanometer resolution, with comparable writing

---

* Corresponding author.
  E-mail address: phyjavk@nus.edu.sg (J.A. van Kan).

speed to that of EBL system, is being built in CIBA. This paper evaluates the performance of the upcoming c-PBW system.

2. Requirements for c-PBW

2.1. Proposed proton energy for c-PBW

The objective of the proposed c-PBW system is to fabricate sub-10 nm structures in 200 nm thick photoresists. For finer patterns, the response of resists is very important and hence the choice of resists becomes critical, for example, 10 nm lines have been achieved in 60 nm thick HSQ using EBL [28]. In an another example, sub-5 nm lines have been fabricated in 25 nm thick HSQ with EBL [29]. As well as for PMMA, 5–7 nm grating lines were successfully patterned at a pitch of 30 nm in a 40 nm thick resist layer [30]. However, for EBL, a thicker resist layer introduces higher electron beam forward scattering and therefore generates more secondary electrons in the resist, resulting in a broadening effect of the structures [31]. In PBW, 19 nm wide lines with a spacing of 80 nm in a 100 nm thick HSQ layer have been demonstrated by a focused 2 MeV proton beam [21].

Pattern dimensions are determined by the response of resist, the beam lateral spread, the beam spot size, and the energy transferred to secondary electrons. Protons are more suitable for fabricating nanostructures in thicker resists. The lateral spread radii of the proton beam for different beam energies within PMMA were simulated using Monte Carlo simulation program SRIM [32], and are shown in Fig. 1. Plots in Fig. 1 were obtained by accounting for 90% of the total incoming protons. As seen from Fig. 1, for 100 keV protons, beam spot size is broadened to 10 nm after passing through 200 nm of PMMA. However, the lateral beam diameter broadening within 200 nm of PMMA is 5 nm for 200 keV protons and 2 nm for 500 keV protons. Taking secondary electrons into account, for 500 keV protons, 90% of energy deposited due to secondary electrons is within 1 nm radial distance from the original proton track [13]. Furthermore, for lower energy protons, secondary electrons will travel even shorter distance due to the reduced energy transferred from protons. Therefore, from a system design perspective, 200 keV protons with a sub-5 nm beam spot size are better suited to fabricate sub-10 nm structures in 200 nm thick PMMA. For thinner PMMA, beam lateral spread and secondary electrons play a less crucial role in beam broadening, and hence the pattern dimensions are dominated by the beam spot size. Therefore, for the c-PBW, a sub-10 nm beam spot size is suf-
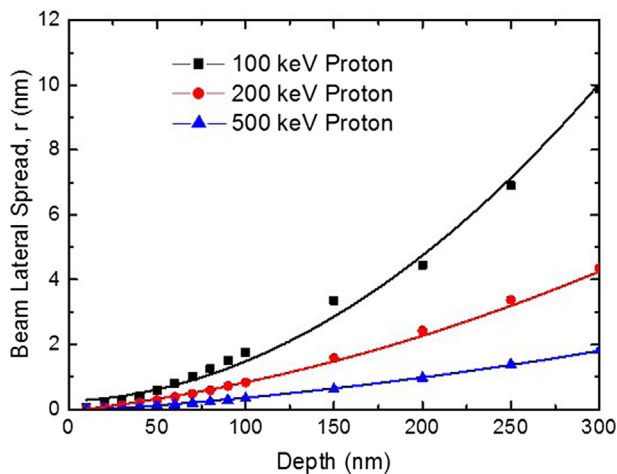
ficient to meet the objective of achieving sub-10 nm structures in 100 nm thick photoresists.

Although a sub-10 nm spot size in one direction has been achieved with the current PBW system [22], the primary limitation of this system is its low reduced brightness resulting in a slow writing speed. This restricts the sub-10 nm focusing capability and also ends up having a low beam current (~0.01 fA) resulting in a low throughput [22]. For EBL, the typical beam current at the image plane is around tens of pA [27], which is 6 orders of magnitude higher than the current PBW system. But the typical dose required for protons in PMMA is 80–150 nC/mm^2 [33], which is 100 times lower than in EBL [34]. Thus in order to make the proposed c-PBW comparable to the EBL in its performance, a high brightness ion source is required that can deliver >0.2 pA of beam current at the image plane.

2.2. Nano-aperture ion source (NAIS)

A nano-aperture ion source (NAIS) [35] has been reported by the Charged Particle Optics group at Delft University of Technology that has the potential to become part of our proposed c-PBW system, to achieve a sub-10 nm beam spot size and faster writing capability. The concept of this NAIS is to extract ions from a small aperture (~100 nm) generated by electron-gas collisions within a sub-micron ionization chamber, as shown schematically in Fig. 2. This dramatically reduces the source size from mm range (as is the case with current PBW system) to the sub-micron range (~100 nm). Once ions are produced inside the ionization chamber, a strong electric field (~10^7 V/m) is applied to extract these ions. Since the ionization chamber spacer is only 100 nm, a small bias voltage (~1 V) is sufficient to generate such a strong electric field, resulting in a minimal ion energy spread (~1 eV).

From the electron-gas collision, the resulting proton beam current density J_p is described as

$$J_p = \sigma J_e N l \tag{1}$$

where J_p and J_e are current densities of protons and injected electron beam respectively, N is the gas density (corresponding to inlet gas pressure P) inside the ionization chamber, l is the spacer length between the two membranes, and σ is the electron impact gas ionization cross section. The energy of the injected electrons was chosen to be 1 keV, a trade-off between currently available electron beam systems and ionization cross section [35,36]. For hydrogen: the electron impact ionization cross section, σ (with 1 keV electrons) to generate H$_2^+$ and H$^+$ is 2.02×10^{-17} cm^2 and 1.19×10^{-18} cm^2 respectively [36].

For a planar ion source emitter, reduced brightness B_r is given as [37]

Fig. 1. Proton beam lateral spread radii in PMMA for 100 keV, 200 keV and 500 keV calculated from SRIM. These plots were obtained by accounting for 90% of the total incoming protons.
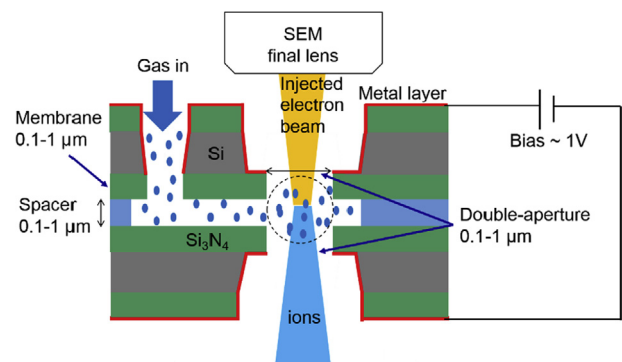

Fig. 2. Schematic of NAIS configuration and its dimensions.

$$B_r = \frac{eJ_P}{\pi kT} \qquad (2)$$

where e is the electric charge, k is the Boltzmann constant, and T is the operating temperature (in our case, it is room temperature $\sim$300 K). In order to minimize ion-gas collisions for better beam brightness [35], the ionization chamber spacer length, l, is set to be equal to that of the gas mean free path λ. Thus the ionization efficiency for protons is given by,

$$\frac{J_p}{J_e} = \frac{\sigma(H^+)}{\sqrt{2}\pi D^2} \qquad (3)$$

where D is the effective molecular diameter, here 0.268 nm for hydrogen [38].

As mentioned above, we choose 1 keV electrons to ionize the gas. These electrons will be injected into the ionization chamber using a Schottky electron emitter, which is capable of delivering few μA electrons with a beam spot size of around 100 nm [27]. According to Eqs (2) and (3), these injected electrons can produce proton beam with a reduced brightness, B_r of 10^6 A/(m² srV) with 500 pA current through a 60 nm virtual source size. In CIBA, we have successfully developed a process to fabricate this new NAIS ion source by utilizing microelectromechanical systems (MEMS) technology [39]. The reduced brightness of this prototype NAIS, when tested with argon gas at 700–800 mbar, was reported as 750–800 A/(m² srV) with 53 pA axial beam current ([40], [Xu et al. in these proceedings]). This reduced brightness of NAIS was primarily limited by the low electron beam brightness from the SEM and also due to the large spacer used in the NAIS ionization chamber. A modified NAIS is under development, at CIBA, to obtain higher reduced brightness of proton beam.

3. Evaluation of c-PBW system with NAIS

3.1. Layout of the c-PBW system

Here we propose a c-PBW system that will employ this promising high brightness NAIS for sub-10 nm lithography. As discussed in Section 2.2, a NAIS with 10^6 A/(m² srV) reduced brightness, 500 pA current, and 60 nm virtual source size is adopted to evaluate the c-PBW system performance. The layout of the proposed c-PBW system is shown in Fig. 3. Protons are generated by electron-gas collisions, in NAIS, and extracted with a tunable extraction voltage in the range of −5 kV to −10 kV. Subsequently, a condenser lens is used to shape the beam. The converged beam is then passed through an acceleration column, where it gains a final energy of 200 keV. A collimator aperture is used to prevent further transmission of high angular scattered ions, while mostly allowing less divergent ions to enter into the focusing lenses. An electrostatic scanner is used, before the focusing lens system, to scan the beam after it is collimated. Three or four electromagnetic quadrupole lenses are employed to focus the beam into the end-station with sub-10 nm resolution. Considering a 2 μm inaccuracy in sample positioning (at image plane), with a preset upper limit of the beam half angle α to 0.25 mrad, will ensure that the beam broadening is not more than 1 nm. The reduced brightness is given as [41],

$$B_r = \frac{I_P}{A_0 \Omega V} \approx \frac{I_P}{\frac{\pi}{4} d_P^2 \pi \alpha^2 V} \qquad (4)$$

where I_P (>0.2 pA) is the proton beam current, A_0 is the beam area, d_P (<10 nm) is the beam diameter at the focal plane, Ω is the solid angle, α (<0.25 mrad) is the beam half-angle divergence, and V (200 kV) is the beam terminal voltage at the image plane. In order to achieve fast writing speed using the c-PBW system, with the limitation explained above, we require an ion source with a reduced brightness of more than 5×10^4 A/(m² srV), which NAIS possess.
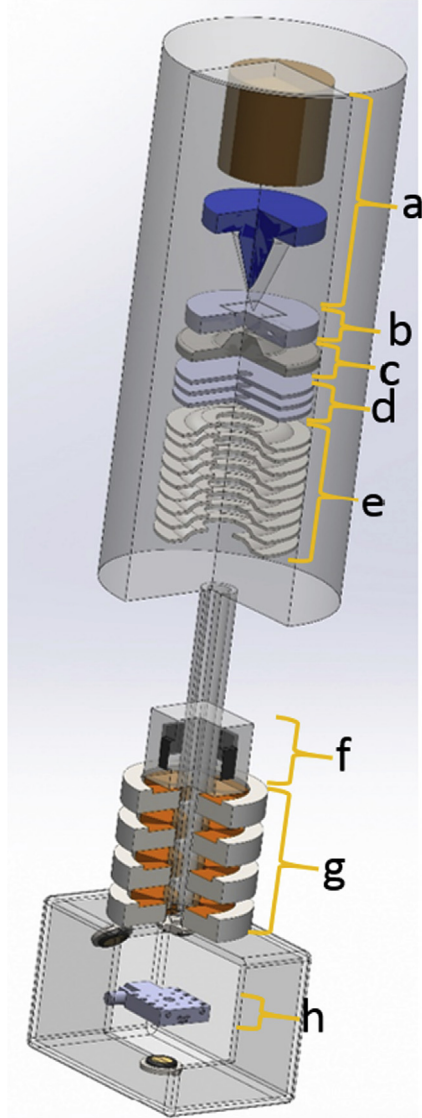

Fig. 3. Schematic of a proposed c-PBW system for sub-10 nm lithography with 200 kV terminal voltage, integrated with a NAIS. (a) Electron injector, (b) NAIS, (c) extractor, (d) condenser lens, (e) acceleration tube, (f) electrostatic scanner, (g) focusing lenses, (h) sample stage.

3.2. Lens configuration and probe beam evaluation of c-PBW system

Apart from the need for a high source reduced brightness, optimizing the focusing lens configuration plays a critical role in determining the capability to reach sub-10 nm proton beam resolution. Particle Beam Optics Laboratory 3.0 (PBO Lab) [42] is used to study the focusing capability of different lens configurations. The two commonly used lens configurations: the low excitation Russian quadruplet [43] and the spaced Oxford triplet [44] configurations are shown in Fig. 4. The Russian quadruplet configuration has the same demagnification in both X and Y, while the spaced Oxford triplet configuration has different demagnifications in X and Y. Four magnetic lenses make up the Russian quadruplet configuration, where the separation between all lenses is fixed at 25 mm with the exception of lens 2 and 3 ($L_{2,3}$). $L_{2,3}$ is varied to evaluate the focusing performance of this configuration. For the spaced Oxford triplet configuration, three magnetic lenses were used with a fixed separation of 25 mm between lens 2 and 3. The distance between lens 1 and 2 ($L_{1,2}$) is varied to investigate the focusing performance.
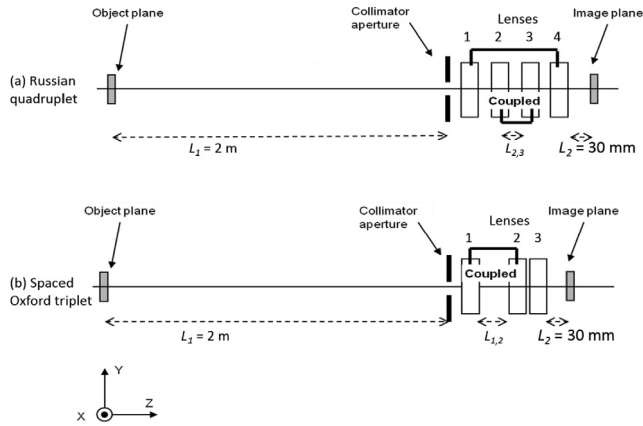
Fig. 4. Layout of focusing lens configurations. (a) Russian quadruplet configuration with 4 lenses and (b) spaced Oxford triplet configuration with 3 lenses.

In the c-PBW system, protons are extracted and accelerated to 200 keV to reach the object plane. In our simulations, we have considered the object beam size (d_v) to be the same as virtual source size for simplicity. The distance between object plane and focusing lens 1, L_1, is set to be 2 m for this c-PBW system. The working distance L_2 is fixed at 30 mm for both lens configurations. A 200 keV proton beam is considered to have 2 eV beam energy spread, caused by the combined effect of the NAIS source energy spread (<1 eV) and <10 ppm acceleration power instability (<2 V for 200 kV). The instability of the magnetic field from the focus lens is 1 ppm.

A systematic approximation by root-power-sum algorithm for full width 90% (FW90, the width including 90% of proton beam current) proton beam diameter d_p at image plane is described as [45],

$$d_p = \left\{ \left[d_I^{1.3} + (d_A^4 + d_C^4)^{1.3/4} \right]^{2/1.3} + d_S^2 \right\}^{1/2} \qquad (5)$$

where d_I is demagnified virtual source size, and is given by

$$d_I = \frac{d_v}{Dem} = \frac{2}{\pi} \sqrt{\frac{I_p}{B_r V}} \frac{1}{\alpha} \qquad (6)$$

(where d_v is the proton virtual source diameter, Dem is the demagnification of the focusing lens) d_A, d_S, and d_C are the contributions from diffraction aberration, spherical aberration, and chromatic aberration, respectively. The contribution from the diffraction aberration is negligible, because the de Broglie wavelength of 200 keV proton is small ($\sim 6 \times 10^{-14}$ m). The contribution from spherical and chromatic aberrations are,

$$d_S = 0.18 C_s \alpha_e^3 \qquad (7)$$

$$d_C = 0.6 C_C \frac{\delta U}{V} \alpha_e \qquad (8)$$

α_e is the proton beam half angle before entering the focusing lens, C_s and C_c are the spherical and chromatic aberrations, and δU is the beam energy spread.

PBO Lab calculates the lens demagnification (Dem), chromatic (C_C), and spherical (C_s) aberrations. These parameters are expressed in two orthogonal directions (X and Y) for an astigmatic lens system. The characteristic values obtained from PBO Lab for Russian quadruplet configuration are summarized in Table 1. The coulomb effect is neglected here, and will be discussed in detail in Section 3.3.

The final probe beam FW90 width at the image plane is shown in Fig. 5a and b, as a function of $L_{2,3}$ and $L_{1,2}$, respectively. The most

Table 1
Parameters obtained from PBO Lab with the Russian quadruplet configuration at $L_{2,3}$ = 25 mm.

Proton beam energy		200 keV
Object plane to lens distance		2 m
Working distance		30 mm
Demagnification, Dem	$1/\langle x\|x\rangle$	10.5
	$1/\langle y\|y\rangle$	10.5
Chromatic aberration, C_C	$\langle x\|x'd\rangle$	2872 μm/mrad
	$\langle y\|y'd\rangle$	5776 μm/mrad
Spherical aberration, C_s	$\langle x\|x'^3\rangle$	−1.414 μm/mrad³
	$\langle x\|x'y'^2\rangle$	−8.081 μm/mrad³
	$\langle y\|y'\rangle$	−8.689 μm/mrad³
	$\langle y\|x'^2y'\rangle$	−8.081 μm/mrad³

ideal lens distances for obtaining sub-10 nm beam spot sizes in Russian quadruplet and spaced Oxford triplet are $L_{2,3}$ = 25 mm and $L_{1,2}$ = 105 mm, respectively. With the preferred lens spacing for both configurations, beam widths and divergences are examined according to different beam currents, as shown in Fig. 5c–f. From Fig. 5c, we can see that the beam spot size remains sub-10 nm up to 15 pA. The different beam currents are obtained by changing the collimator aperture, resulting in the change of beam half angle α. From Fig. 5d, it is clear that in order not to exceed the preset upper limit of beam half angle α (0.25 mrad), the beam current cannot exceed 2 pA for the Russian quadruplet lens configuration.

Since spaced Oxford triplet configuration has different demagnification in X and Y directions, there are two different preset upper limits for the beam half angle, α_x and α_y respectively. From Fig. 5f, we can have a beam current of 0.5 pA while maintaining α_y well below 0.25 mrad. Whereas due to the high demagnification in X direction, the upper limit of α_x can be increased up to 2 mrad (still maintaining a sub-10 nm focus in X, see Fig. 5e), while yielding a beam current of 0.5 pA. Table 2 summarizes the performance of these two lens configurations for the c-PBW system, compared with the current PBW and EBL. It shows a promising high-throughput for the c-PBW system in the sub-10 nm regime that is faster than in EBL.

In lithography, the possibility of having a large scan size ($\sim$10's μm) in the image plane is generally desirable. The current PBW in CIBA employs an electrostatic scanning system with X and Y scanning plates [25]. The off-axis aberration can deteriorate the final beam quality, and enlarge the beam size. In the PBO simulation, a scanner is located 20 mm upstream from the first lens for both lens configurations. As shown in Fig. 6, the Russian quadruplet lens configuration can achieve sub-10 nm beam size with a 400×400 μm² scan size, while the spaced Oxford triplet lens configuration can only have a 30×30 μm² scan size, which is limited by the larger off-axis aberration (all simulations were performed with 0.2 pA).

3.3. Coulomb effect of c-PBW system

An ion beam is not only affected by external fields but also influenced by the charged particles that introduce fields with neighboring ions, named as Coulomb effects. Generally, Coulomb effects consist of three different type of effects: a space charge effect, a Boersch effect, and a trajectory displacement effect [27]. Space charge effect is a deflection of a charged particle acted upon by the self-field generated by the beam. Usually, for a round beam with uniform distribution, space charge effect can be compensated by the external lens due to the linear force in the transverse plane, and therefore neglected. Boersch effect and trajectory displacement effect are stochastic effects which are introduced by pairwise interactions between charged particles. Trajectory displace-
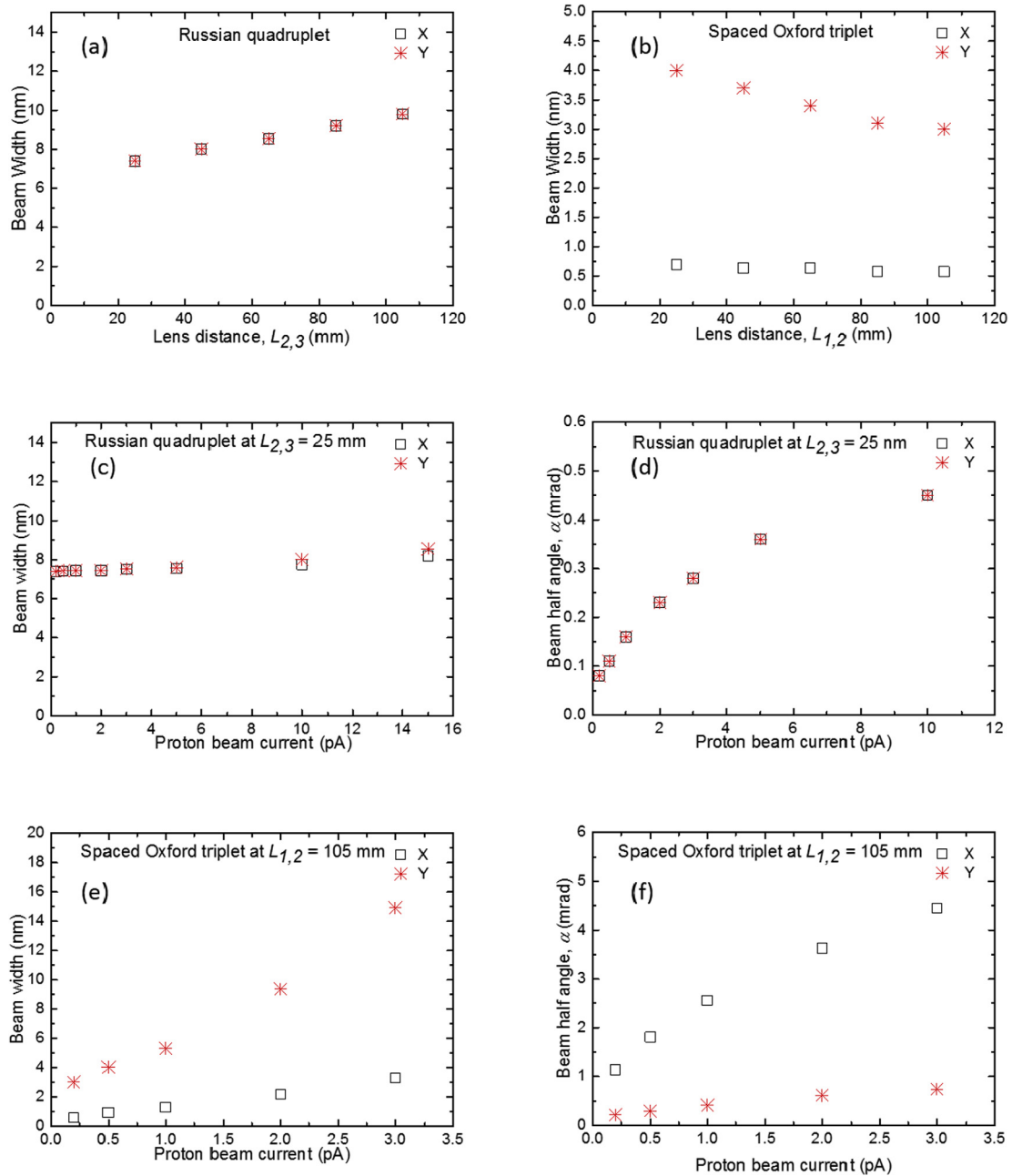
Fig. 5. Proton beam FW90 widths in X and Y directions with the variation of lens distance for (a) Russian quadruplet configuration, (b) spaced Oxford triplet configuration, (c) proton beam widths in X and Y directions with the variation of beam current, (d) proton beam divergence α with the variation of beam current, for $L_{2,3}$ = 25 mm Russian quadruplet lens configuration, (e) proton beam widths in X and Y directions with the variation of beam current and (f) proton beam divergence α with the variation of beam current, for $L_{1,2}$ = 105 mm spaced Oxford triplet lens configuration.

Table 2
Summary of 200 kV c-PBW with different lens configurations, to write a 10 nm × 1 mm line on PMMA, comparing with current PBW and EBL.

| Lithographic probe	c-PBW		Current PBW [22]	EBL [27,34]
Beam virtual source diameter (nm)	60	60	~2 mm	
Lens configuration	Russian quadruplet	Spaced Oxford triplet	Spaced Oxford triplet	
Lens spacing (mm)	$L_{2,3}$ = 25	$L_{2,3}$ = 105		
Beam exit current from ion source (pA)	500	500	~µA	
Beam energy (keV)	200	200	2000	~10's
Beam size at image plane (nm^2)	7.5 × 7.5	0.9 × 4	9.3 × 32	5 × 5
Beam current at image plane (pA)	2	0.5	0.013	20
Beam half angle at image plane (mrad)	0.23 × 0.23	1.8 × 0.3	1.7 × 0.3	
Beam reduced brightness (A/(m^2 srV))	~1 × 10^6	~1 × 10^6	~10	~10^7
Writing time (second)	0.5	2	100	5
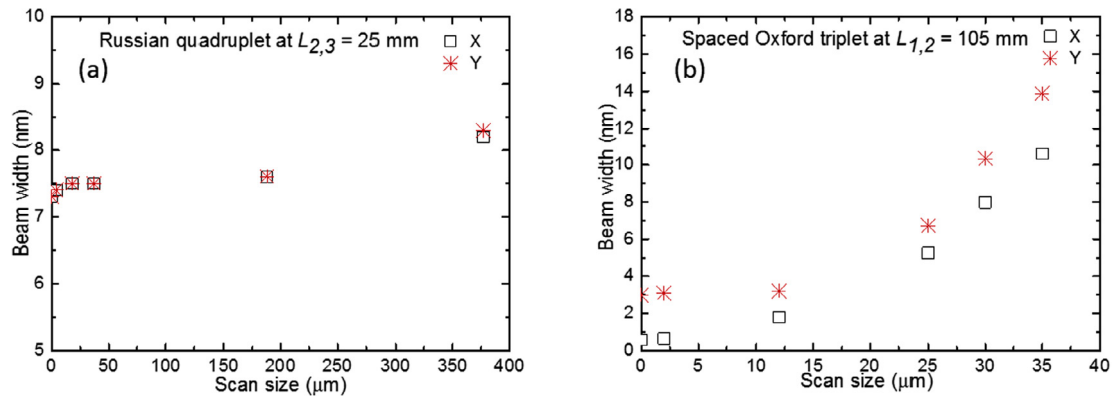
Fig. 6. Proton beam widths in X and Y directions as a function of scan size, (a) $L_{2,3}$ = 25 mm in Russian quadruplet lens configuration, (b) $L_{1,2}$ = 105 mm in spaced Oxford triplet lens configuration.

ment creates more spread towards the transverse energy of the beam, which in turn degrades the beam brightness. Meanwhile, the longitudinal beam energy gets broadened towards the thermodynamic equilibrium with the change of transverse energy, and this causes the total beam energy spread known as Boersch effect. These stochastic effects cannot be compensated by adjusting external focus fields. In most scenarios, at the high current density region, which is normally located at the source part [46], stochastic Coulomb effects can be important. To surmount the Coulomb effect in the source region, a stronger electric field is applied in order to reduce the interaction time. This will generally lead to a larger energy spread. However, in the NAIS setup, a strong field is generated across a sub-micron spacer requiring a small bias potential difference ($\sim$1 V). This NAIS geometry limits the energy spread to less than 1 eV. Considering a typical ionization chamber designed for a Schottky electron injector, the electric field inside the chamber is 10^7 V/m. This electric field will ensure that all the ions generated in the ionization chamber are guided towards the extraction plane. In this scenario the time taken by H^+ and H_2^+ to escape from the source is less than 100 ps. With such a flight time, there is only one ion expected to reside in the ionization chamber at a given point of time (this assumption is valid for ion currents up to $\sim$2 nA [35]), and therefore the Coulomb interactions can be neglected inside the ion source.

4. Outlook and conclusion

The schematic of developing a compact sub-10 nm level PBW system has been briefly discussed. The c-PBW is designed for 200 kV, which is capable for patterning sub-10 nm structures in 200 nm thick PMMA. For obtaining fast writing speed comparable to EBL, a NAIS is employed for this c-PBW system. The NAIS has the potential to deliver protons with 10^6 A/(m^2 srV) brightness, which is 5 orders of magnitude larger than current PBW system and can dramatically increase the throughput. With this ideal NAIS, the lens configuration and beam quality are evaluated for the c-PBW system. Both, Russian quadruplet ($L_{2,3}$ = 25 mm) and spaced Oxford triplet ($L_{1,2}$ = 105 mm) lens configurations are capable of focusing the beam down to a sub-10 nm spot size with a faster writing speed. The Russian quadruplet lens configuration has the ability to deliver 2 pA probe current with 7.5 × 7.5 nm^2 spot size, whereas spaced Oxford triplet can deliver 0.5 pA with 0.3 × 4 nm^2 spot size. Both configurations can match the writing speed to that of an EBL system with sub-10 nm beam spot size. Calculation shows that a sub-10 nm focused beam can be scanned over an area of 400 × 400 μm^2 with the Russian quadruplet lens configuration and 30 × 30 μm^2 with the spaced Oxford triplet lens configuration.

The typical beam scan size for EBL is a few 10's μm [47,48]. Both lens configurations for the c-PBW system can provide comparative scan area as in EBL at high resolution writing mode. For writing a large area, a high-precision stage can be employed in stitching mode. We have also shown that in the proposed c-PBW system, the Coulomb effect is negligible when operated with $\sim$2 nA source current. While these design considerations of a c-PBW system are a conservative estimate, they already suggest a competitive writing speed coupled with minimal proximity effect.

References

[1] Y. Wang, P. Malar, J.A. van Kan, Resist evaluation for proton beam writing, Ni mold fabrication and nano-replication, Microsyst. Technol. 20 (2014) 2079–2088.

[2] J.A. van Kan, P. Malar, Y. Wang, Resist materials for proton beam writing: a review, Appl. Surf. Sci. 310 (2014) 100–111.

[3] J.A. van Kan, A.A. Bettiol, F. Watt, Three-dimensional nanolithography using proton beam writing, Appl. Phys. Lett. 83 (2003) 1629–1631.

[4] J.A. van Kan, A.A. Bettiol, F. Watt, Proton beam writing of three-dimensional nanostructures in hydrogen silsesquioxane, Nano Lett. 6 (2006) 579–582.

[5] F. Menzel, D. Spemann, S. Petriconi, J. Lenzner, T. Butz, Proton beam writing of submicrometer structures at LIPSION, Nucl. Instrum. Methods Phys. Res., Sect. B 260 (2007) 419–425.

[6] V. Auzelyte, M. Elfman, P. Kristiansson, C. Nilsson, J. Pallon, N.A. Marrero, M. Wegdén, Exposure parameters for MeV proton beam writing on SU-8, Microelectron. Eng. 83 (2006) 2015–2020.

[7] J. Simčič, P. Pelicon, Z. Rupnik, M. Mihelič, A. Razpet, D. Jenko, M. Maček, 3D micromachining of SU-8 polymer with proton microbeam, Nucl. Instrum. Methods Phys. Res., Sect. B 241 (2005) 479–485.

[8] I. Rajta, I. Gomez-Morilla, M. Abraham, A. Kiss, Proton beam micromachining on PMMA, Foturan and CR-39 materials, Nucl. Instrum. Methods Phys. Res., Sect. B 210 (2003) 260–265.

[9] P. Mistry, I. Gomez-Morilla, G. Grime, R. Webb, C. Jeynes, R. Gwilliam, A. Cansell, M. Merchant, K. Kirkby, Proton beam lithography at the University of Surrey's Ion Beam Centre, Nucl. Instrum. Methods Phys. Res., Sect. B 242 (2006) 387–389.

[10] M. Cutroneo, V. Havranek, A. Mackova, V. Semian, L. Torrisi, L. Calcagno, Micro-patterns fabrication using focused proton beam lithography, Nucl. Instrum. Methods Phys. Res., Sect. B 371 (2016) 344–349.

[11] N. Uchiya, T. Harada, M. Murai, H. Nishikawa, J. Haga, T. Sato, Y. Ishii, T. Kamiya, Micro-machining of resists on silicon by proton beam writing, Nucl. Instrum. Methods Phys. Res., Sect. B 260 (2007) 405–408.

[12] R. Tsuchiya, H. Nishikawa, Fabrication of silica-based three-dimensional structures by changing fluence using proton beam writing, Trans. Mater. Res. Soc. Jpn. 36 (2011) 325–328.

[13] C. Udalagama, A.A. Bettiol, F. Watt, Stochastic spatial energy deposition profiles for MeV protons and keV electrons, Phys. Rev. B 80 (2009) 224107.

[14] J.A. van Kan, P. Shao, K. Ansari, A.A. Bettiol, T. Osipowicz, F. Watt, Proton beam writing: a tool for high-aspect ratio mask production, Microsyst. Technol. 13 (2007) 431–434.

[15] F. Watt, M.B. Breese, A.A. Bettiol, J.A. van Kan, Proton beam writing, Mater. Today 10 (2007) 20–29.

[16] J.A. van Kan, J. Sanchez, B. Xu, T. Osipowicz, F. Watt, Resist materials for proton micromachining, Nucl. Instrum. Methods Phys. Res., Sect. B 158 (1999) 179–184.

[17] Q. An, C. Cheng, S.K. Vanga, A.A. Bettiol, F. Chen, Proton beam writing of chalcogenide glass: a new approach for fabrication of channel waveguides at telecommunication O and C bands, J. Lightwave Technol. 32 (2014) 3763–3767.

[18] J.A. van Kan, P. Shao, Y. Wang, P. Malar, Proton beam writing a platform technology for high quality three-dimensional metal mold fabrication for nanofluidic applications, Microsyst. Technol. 17 (2011) 1519–1527.

[19] W. Yue, S.-Y. Chiam, Y. Ren, J.A. van Kan, T. Osipowicz, L. Jian, H.O. Moser, F. Watt, The fabrication of x-ray masks using proton beam writing, J. Micromech. Microeng. 18 (2008) 085010.

[20] X. Chen, C.-B. Chen, C.N. Udalagama, M. Ren, K.E. Fong, L.Y.L. Yung, P. Giorgia, A.A. Bettiol, F. Watt, High-resolution 3D imaging and quantification of gold nanoparticles in a whole cell using scanning transmission ion microscopy, Biophys. J. 104 (2013) 1419–1425.

[21] Y. Yao, P.S. Raman, J.A. van Kan, Orthogonal and fine lithographic structures attained from the next generation proton beam writing facility, Microsyst. Technol. 20 (2014) 2065–2069.

[22] Y. Yao, J.A. van Kan, Automatic beam focusing in the 2nd generation PBW line at sub-10nm line resolution, Nucl. Instrum. Methods Phys. Res., Sect. B 348 (2015) 203–208.

[23] C. Moak, H. Reese, W. Good, Design and operation of a radio-frequency ion source for particle accelerators, Nucleonics 9 (1951) 18–23.

[24] F. Watt, J.A. van Kan, I. Rajta, A.A. Bettiol, T. Choo, M. Breese, T. Osipowicz, The National University of Singapore high energy ion nano-probe facility: performance tests, Nucl. Instrum. Methods Phys. Res., Sect. B 210 (2003) 14–20.

[25] J.A. van Kan, P. Malar, A.B. De Vera, The second generation Singapore high resolution proton beam writing facility, Rev. Sci. Instrum. 83 (2012) 02B902.

[26] C. Hagen, E. Fokkema, P. Kruit, Brightness measurements of a gallium liquid metal ion source, J. Vac. Sci. Technol., B 26 (2008) 2091–2096.

[27] J. Orloff, Handbook of Charged Particle Optics, CRC press, 2008.

[28] X. Chen, T. Zhang, V. Constantoudis, S.-L. Zhang, Z. Zhang, Aged hydrogen silsesquioxane for sub-10 nm line patterns, Microelectron. Eng. 163 (2016) 105–109.

[29] J.K. Yang, B. Cord, H. Duan, K.K. Berggren, J. Klingfus, S.-W. Nam, K.-B. Kim, M.J. Rooks, Understanding of hydrogen silsesquioxane electron resist for sub-5-nm-half-pitch lithography, J. Vac. Sci. Technol., B 27 (2009) 2622–2627.

[30] W.W. Hu, K. Sarveswaran, M. Lieberman, G.H. Bernstein, Sub-10 nm electron beam lithography using cold development of poly (methylmethacrylate), J. Vac. Sci. Technol., B 22 (2004) 1711–1716.

[31] A. Grigorescu, C. Hagen, Resists for sub-20-nm electron beam lithography with a focus on HSQ: state of the art, Nanotechnology 20 (2009) 292001.

[32] J.F. Ziegler, J.P. Biersack, The stopping and range of ions in matter, Treatise on Heavy-Ion Science, Springer, 1985.

[33] J.A. van Kan, A.A. Bettiol, S. Chiam, M. Saifullah, K. Subramanian, M. Welland, F. Watt, New resists for proton beam writing, Nucl. Instrum. Methods Phys. Res., Sect. B 260 (2007) 460–463.

[34] M. Yan, S. Choi, K. Subramanian, I. Adesida, The effects of molecular weight on the exposure characteristics of poly (methylmethacrylate) developed at low temperatures, J. Vac. Sci. Technol., B 26 (2008) 2306–2310.

[35] D.S. Jun, V.G. Kutchoukov, P. Kruit, Ion beams in SEM: an experiment towards a high brightness low energy spread electron impact gas ion source, J. Vac. Sci. Technol., B 29 (2011) 06F603.

[36] H. Straub, P. Renault, B. Lindsay, K. Smith, R. Stebbings, Absolute partial cross sections for electron-impact ionization of H_2, N_2, and O_2 from threshold to 1000 eV, Phys. Rev. A 54 (1996) 2146.

[37] K. Smith, Principles of electron optics—volume 2: applied geometrical optics. By PW Hawkes and E. Kasper, J. Microsc. 165 (1992) 189–190.

[38] A. Roth, Vacuum Technology, Elsevier, 2012.

[39] N. Liu, P.S. Raman, X. Xu, H.M. Tan, A. Khursheed, J.A. van Kan, Development of ion sources: towards high brightness for proton beam writing applications, Nucl. Instrum. Methods Phys. Res., Sect. B 348 (2015) 23–28.

[40] N. Liu, X. Xu, R. Pang, P.S. Raman, A. Khursheed, J.A. van Kan, Brightness measurement of an electron impact gas ion source for proton beam writing applications, Rev. Sci. Instrum. 87 (2016) 02A903.

[41] A.V. Crewe, Optimization of small electron probes, Ultramicroscopy 23 (1987) 159–167.

[42] AccelSoft Inc. Particle Beam Optics Laboratory 3.0 (PBO Lab). http://www.ghga.com/accelsoft/pbolab.html.

[43] F. Watt, G.W. Grime, Principles and Applications Of High-Energy Ion Microbeams, 1987.

[44] G.W. Grime, F. Watt, Beam Optics of Quadrupole Probe-Forming Systems, Hilger, 1984.

[45] J. Barth, P. Kruit, Addition of different contributions to the charged particle probe size, Optik 101 (1996) 101–109.

[46] J. Orloff, L. Swanson, M. Utlaut, High Resolution Focused Ion Beams: FIB and its Applications: The Physics of Liquid Metal Ion Sources and Ion Optics and Their Application to Focused Ion Beam Technology, Springer Science & Business Media, 2003.

[47] C. Vieu, F. Carcenac, A. Pepin, Y. Chen, M. Mejias, A. Lebib, L. Manin-Ferlazzo, L. Couraud, H. Launois, Electron beam lithography: resolution limits and applications, Appl. Surf. Sci. 164 (2000) 111–117.

[48] Centre for Advanced 2D Materials and Graphene Research Centre, National University of Singapore. Jeol JBX-6300FS Electron Beam Lithographer Specifications. https://graphene.nus.edu.sg/content/jeol-electron-beam-lithographer-specifications.